Polycomb Group Protein Enhancer of Zeste 2 Is an Oncogene That Promotes the Neoplastic Transformation of a Benign Prostatic Epithelial Cell Line

Breanne D.W. Karanikolas,[1,2] Marxa L. Figueiredo,[4] and Lily Wu[1,3]

[1]Department of Molecular and Medical Pharmacology, [2]Molecular Biology Interdepartmental Program, and [3]Department of Urology, Crump Institute for Molecular Imaging, and Jonsson Comprehensive Cancer Center, David Geffen School of Medicine, University of California at Los Angeles, Los Angeles, California and [4]Department of Comparative Biomedical Sciences, School of Veterinary Medicine, Louisiana State University Baton Rouge, Louisiana

Abstract

Polycomb group protein enhancer of zeste 2 (EZH2) is a master regulatory protein that plays a critical role in development as part of the polycomb repressive complex 2. Polycomb repressive complex 2 controls numerous cell cycle and regulatory genes through trimethylation of histone 3, which results in chromatin condensation and transcriptional silencing. EZH2 overexpression has been correlated with high incidence of more aggressive, metastatic prostate cancers. Although this correlation means EZH2 could prove valuable as a biomarker in clinical settings, the question remains whether EZH2 is actually responsible for the initiation of these more aggressive tumor types. In this study, EZH2-mediated neoplastic transformation of the normal prostate epithelial cell line benign prostate hyperplasia 1 (BPH1) was confirmed by *in vivo* tumor growth and *in vitro* colony formation. Furthermore, EZH2 transformation resulted in increased invasive behavior of BPH1 cells, indicating that EZH2 may be responsible for aggressive behavior in prostate cancers. BPH1 was also transformed with the classic oncogenes myristoylated Akt and activated Ras(V12) to allow phenotype comparisons with the EZH2-transformed cells. This study marks the first demonstration of neoplastic transformation in prostate cells mediated by EZH2 and establishes that EZH2 possesses stronger transforming activity than Akt but weaker activity than activated Ras. (Mol Cancer Res 2009;7(9):1456–65)

Received 3/20/09; revised 6/18/09; accepted 7/6/09; published OnlineFirst 9/1/09.
Grant support: University of California at Los Angeles Specialized Program of Research Excellence in Prostate Cancer Career Development Award (B.D.W. Karanikolas).
The costs of publication of this article were defrayed in part by the payment of page charges. This article must therefore be hereby marked *advertisement* in accordance with 18 U.S.C. Section 1734 solely to indicate this fact.
Note: Supplementary data for this article are available at Molecular Cancer Research Online (http://mcr.aacrjournals.org/).
Requests for reprints: Lily Wu, Departments of Molecular and Medical Pharmacology and Urology, University of California at Los Angeles, CHS 33-118, Box 951735, Los Angeles, California 90095-1738. Phone: 310-825-8511; Fax: 310-206-5343. E-mail: LWu@mednet.ucla.edu
Copyright © 2009 American Association for Cancer Research.
doi:10.1158/1541-7786.MCR-09-0121

Introduction

Polycomb group (PcG) protein enhancer of zeste 2 (EZH2) was first identified for its master regulatory role over the homeobox genes during development. By controlling spatial and temporal expression of various developmental genes, EZH2 and its family members determine body patterning and cell fate (1, 2). Within the polycomb group family exist two complexes: polycomb repressive complex 1 (PRC1) and polycomb repressive complex 2 (PRC2), the latter of which is composed of EZH2 and its binding partners EED and Su(z)12 (3, 4). PRC2 is expressed by proliferating cells and is responsible for silencing target genes through trimethylation of lysine 27 on histone 3 (5-9). EZH2 is the member of PRC2 responsible for the methyltransferase activity via the COOH-terminal SET domain (10).

EZH2 was implicated in cancer aggression when it was found to be expressed at very high levels in proliferating mantle cell lymphoma samples (11). Soon thereafter, a gene array comparing benign and metastatic prostate cancer samples found that EZH2 was consistently overexpressed in metastatic cancer (12). Furthermore, EZH2 expression levels were found to be predictive of metastatic behavior in early-stage, organ-confined prostate cancers. Subsequently, EZH2 was found to be overexpressed in the more aggressive forms of breast (13, 14), endometrium (15), melanoma (16), myeloma (17), and gastric (18) cancers, to name a few (19).

Additional evidence regarding EZH2 and its relationship to prostate cancer aggression continued to inundate the field. *In situ* hybridization experiments on advanced-stage prostate cancer samples found that, in many cases, EZH2 overexpression was possibly due to gene amplification (20) or a loss of microRNA-mediated inhibition (21). EZH2 was also validated as a biomarker that could be used to determine risk of prostate cancer recurrence in patients (22-24). Furthermore, it was confirmed that EZH2 was involved in maintaining proliferation and invasive behavior of some prostate cancer cell lines (25). Despite this abundance of data on prostate cancer and prostate cancer cell lines, little work has been done to examine the role of EZH2 in cancer initiation. One study showed that EZH2 promoted transformation of breast epithelial cells (26), but a parallel work in prostate epithelial cells has not been done. However, tissue-specific differences between breast and prostate cells indicate that a transformation study in prostate cells is warranted. For instance, androgen receptor, which is critical

for the growth of prostate cells and not expressed by breast cells, is recruited to target genes by the histone demethylase responsible for reversing the histone modification made by EZH2 (27), indicating the strong possibility of alternative pathways and mechanisms that may be activated in prostate cells.

Benign prostate hyperplasia 1 (BPH1) is an epithelial cell line that was derived from a tissue biopsy and immortalized using SV40 large T antigen (28). Following immortalization, BPH1 remained nontransformed and has been used extensively as a cell line representing a more normal prostate epithelium (29, 30). BPH1 has become a widely accepted model in which to study the initiation of prostate cancer. The cell line has been transformed using coculture with cancer-associated fibroblasts (31, 32) and with urogenital sinus mesenchyme treated with testosterone and estradiol (33). The transformed sublines of BPH1 have then been studied as early-stage versions of prostate cancer.

Two well-known and classic oncogenes are myristoylated Akt and Ras(V12), which are both constitutively active. Akt has been confirmed to play a signaling role in prostate cancer growth (34, 35) and promotes the development of precancerous prostatic intraepithelial neoplasia in a transgenic model (36). Ras is most often found in cancers in a mutated, constitutively active form that provides constant mitogenic and growth signaling (ref. 37; reviewed in refs. 38, 39). Although this is also predominantly true for prostate cancer, some studies have determined that simply overexpressing Ras can cause cancer phenotypes (40, 41). Continuous Ras pathway signaling, either by mutation or by overexpression, results in less dependency on androgen receptor signaling in prostate cancer cells (42). This most likely contributes to development of late-stage hormone-refractory prostate cancer (43).

In this study, EZH2 was overexpressed in the normal prostatic epithelial cell line BPH1 to investigate the effect of EZH2 on prostate cancer initiation. The resulting data suggest that EZH2 is in fact a transforming factor for BPH1 cells, leading to a loss of contact inhibition, an increase in invasive behavior, and tumor growth *in vivo*. Furthermore, this study directly compares EZH2 with the classic oncogenes Akt and Ras, thus allowing the strength of EZH2 as an oncogene in prostate cancer to be rated.

Results

Overexpressed EZH2 in BPH1 Alters H3K27Me3 Levels

The role of EZH2 in prostate cancer aggression has been repeatedly confirmed; however, no data exist on whether EZH2 is involved in the initiation of prostate cancer. It has been shown previously that prostate cancer cell lines express anywhere from 10- to 80-fold more EZH2 compared with normal prostatic epithelia (44). The immortalized but nontransformed epithelial prostate cell line BPH1 was found to express lower levels of EZH2 than various prostate cancer cell lines by both quantitative real-time PCR (qRT-PCR) and Western blot (data not shown). Because EZH2 stability and activity is dependent on binding to EED, the ratio between endogenous EZH2 and EED was also examined. BPH1 cells had ~3-fold higher expression of EED than EZH2 (EED/EZH2 ratio is 2.76; Fig. 1B), implying the presence of unbound EED theoretically available to stabilize additional EZH2 activity. Taken together, these data indicated that BPH1 was an excellent cell line in which to study the effect of EZH2 overexpression.

To overexpress EZH2 in a stable manner, self-inactivating lentiviral vectors were used (45). Self-inactivating lentiviruses are useful for overexpression studies because of their safety and stable integration into the genomes of infected cells. The control lentivirus for this study contained a cytomegalovirus immediate-early (CMV) promoter followed by the encephalomyocarditis virus internal ribosomal entry site (IRES) driving expression of enhanced green fluorescent protein (EGFP; Fig. 1A). Hereafter, the control virus will be called GFP. For EZH2 overexpression, HA-tagged EZH2 was inserted into the lentiviral vector under control of the CMV promoter (Fig. 1A). Following lentiviral transduction, BPH1-EZH2 had ~40 times higher expression of EZH2 compared with BPH1-GFP (EED/EZH2 ratio of 2.2) by qRT-PCR (Fig. 1B). Expression of exogenous EZH2 was also confirmed by Western blot, although significant degradation of the protein product was observed due to saturation of the available EED (EZH2/EED ratio of 10.4; Fig. 1C; Supplementary Fig. S1). By Western blot densitometry, a 65% increase in EZH2 protein over endogenous levels was achieved in BPH1-EZH2 cells compared with BPH1-GFP cells.

To examine the functional consequence induced by EZH2 overexpression, immunocytochemical staining for histone 3 lysine 27 trimethylation (H3K27Me3), a unique histone modification attributed to the EZH2 complex, was done (Fig. 2). Although all cells stained positive for H3K27Me3 due to endogenous EZH2, cells that were overexpressing EZH2 had much higher levels of H3K27Me3 (indicated by brighter red staining; Fig. 2). These results indicate that the overexpression of EZH2 caused a discernible epigenetic modification in the transduced BPH1 cells.

EZH2 Is a Stronger Transforming Factor than Akt

The transforming activity of EZH2 was compared with either the constitutively active myristoylated Akt (46) or activated K-Ras(V12) mutant (47) to evaluate the strength of EZH2 as a transforming factor. Given that Ras is upstream of Akt, with considerably more downstream effectors, it was expected to be a stronger transforming factor than Akt. For these positive controls, BPH1 cells were marked at a multiplicity of infection of 1 with either Akt or K-Ras overexpression lentivirus. Following lentiviral infection, BPH1-Akt cells expressed 30-fold more Akt and BPH1-Ras cells expressed 60-fold more Ras than uninfected BPH1 cells.

Because prior reports have implicated EZH2 in prostate cancer cell line proliferation (25), the mitogenic effects of EZH2 overexpression on BPH1 were investigated. CCK8 proliferation assay, which measures the number of live, metabolizing cells present in a sample, was done on all BPH1 sublines (BPH1-GFP, BPH1-EZH2, BPH1-Ras, and BPH1-Akt). By this method, no discernable differences in proliferative rates were observed (Supplementary Fig. S2). To evaluate the rate of cell death in each BPH1 subline population, lactase dehydrogenase assays were done. Lactase dehydrogenase is a stable cytoplasmic enzyme released into the culture medium on plasma membrane damage in an apoptotic or damaged cell. Uninfected

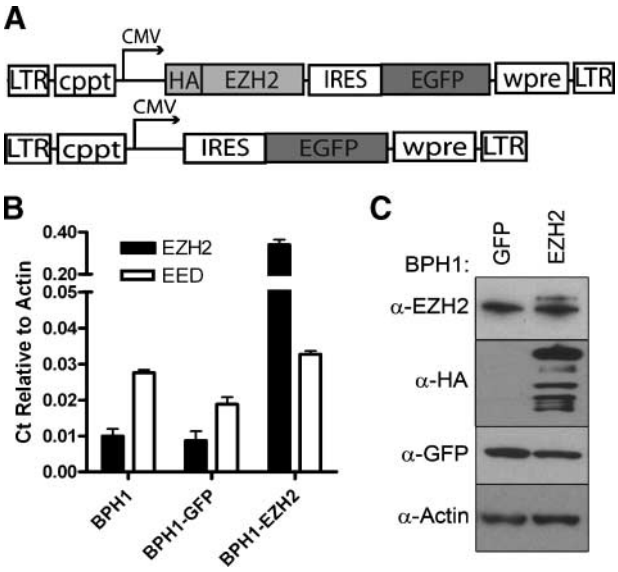

FIGURE 1. Lentiviral schematics and EZH2 overexpression in BPH1. **A.** Schematic diagram of EZH2 overexpression and GFP control lentiviral vectors. *LTR,* long terminal repeat; *cppt,* central polypurine tract; *CMV,* human CMV promoter; *wpre,* woodchuck post-transcriptional regulatory element. **B.** qRT-PCR analysis of EZH2 and EED levels in transduced BPH1 populations. EZH2 overexpression achieved in the BPH1-EZH2 population was 40-fold the endogenous levels. **C.** Western blot analysis of overexpression of EZH2 in BPH1-EZH2 cells. α-EZH2, antibody specific for endogenous and overexpressed EZH2; α-HA, antibody specific for HA-tagged EZH2; α-GFP, antibody specific for GFP protein expression; α-Actin, antibody specific for β-actin used as a loading control. In α-HA panel, the top band represents full-size HA-tagged EZH2. Bottom bands represent degradation of HA-tagged EZH2. Blots shown are cropped for space considerations. Full blots can be seen in Supplementary Fig. S1.

BPH1 and BPH-GFP both had very low levels of cell death by this assay. BPH1-EZH2, BPH1-Akt, and BPH1-Ras all had statistically significant ($P = 0.0006$, 0.006, and 0.000034, respectively) increases in lactase dehydrogenase activity, indicating increased cell turnover commonly associated with a transformed phenotype (Supplementary Fig. S2). Taken in conjunction with the growth assay, it appears that the transformed cells may in fact proliferate more rapidly than the untransformed controls. However, the more rapid proliferation is balanced by a more rapid rate of cell turnover, resulting in a steady state of live cells in BPH1-EZH2, BPH1-Akt, and BPH1-Ras equivalent to the unmarked BPH1.

All BPH1 sublines were plated in a soft-agar transformation assay. Uninfected BPH1 cells plated in soft agar resulted in very few colonies, verifying their nontransformed state (Supplementary Fig. S3). Those spots that were visible were attributed to cells that were clustered at the time of plating. As predicted, both BPH1-Akt and BPH1-Ras cells grew colonies in soft agar. The BPH1-Ras grew into larger (Fig. 3C) and more numerous (Fig. 3B) colonies than BPH1-Akt (Fig. 3A). BPH1-GFP showed no increase in colony-forming activity over the uninfected BPH1 (Fig. 3A; Supplementary Fig. S3). When BPH1-EZH2 was used in the soft-agar transformation assay, the cells were capable of growing sizable colonies. BPH1-EZH2 colonies were larger (Fig. 3C) and more numerous (Fig. 3B) than BPH1-Akt but smaller and less numerous than BPH1-Ras. It was therefore concluded that EZH2 is an oncogene in the sense that it alone is sufficient to cause the neoplastic transformation of an otherwise benign prostate epithelial cell line. Furthermore, EZH2 can be placed within the spectrum of known oncogenes as stronger than Akt but weaker than Ras in transforming capability.

EZH2 Overexpression Causes an Increase in Invasion by BPH1 Cells

To explore the role of EZH2 in aggression, BPH1 sublines were assayed for invasive behavior toward either medium containing 10% fetal bovine serum (FBS; Fig. 4A) or 3T3 conditioned medium (Fig. 4B). For all cell types, the 3T3 conditioned medium stimulated more invasive behavior than the 10% FBS medium (quantified in Table 1). Uninfected BPH1 and BPH1-GFP showed the least and BPH1-Ras showed the greatest amount of invasion (Fig. 4A and B; Supplementary Fig. S3). BPH1-Akt showed a significant increase in invasive behavior compared with BPH1-GFP in the FBS but not the 3T3 assay (Fig. 4C and D). BPH1-EZH2 cells were more invasive than control cells toward both FBS and 3T3 media (Fig. 4A and B). Collectively, the invasive behavior of EZH2-transformed BPH1 was comparable with BPH1-Akt and slightly lower than BPH1-Ras in both 3T3 and FBS assays (Fig. 4A-D).

Oncogene-Induced Tumor Growth in Severe Combined Immunodeficient Mice

A more stringent assay for tumorigenicity is the ability to form a tumor in an *in vivo* environment. Before implantation into severe combined immunodeficient mice, all BPH1 sublines were additionally marked with a *Renilla* luciferase (RLuc)–expressing lentivirus to facilitate monitoring of tumor growth. RLuc signal was verified via optical imaging on day 0 immediately following implantation to confirm that each mouse received an equivalent number of cells (Fig. 5A). Tumor growth was then monitored by optical imaging (data not shown) and caliper measurements (Fig. 5B) until they reached 1 cm or for 12 weeks, whichever occurred first (Fig. 5A). BPH1-Ras tumors ($n = 4$) grew to 1 cm in 3 weeks and BPH1-Akt tumors ($n = 3$) in 12 weeks (Fig. 5C). EZH2-transformed BPH1 tumors ($n = 8$), however, were ~0.6 cm at 12 weeks. Consequently, one subgroup of BPH1-EZH2 tumor-bearing mice ($n = 4$) were monitored through 28 weeks of growth, when the tumors reached 1 cm (Fig. 5C). At the 12-week endpoint, BPH1-Ras, BPH1-Akt, and BPH1-EZH2 tumor growth was confirmed by an increase in mass compared with the BPH1-GFP control ($n = 4$) group (Fig. 5D).

To confirm the functionality of lentivirally introduced EZH2, qRT-PCR was done on tumors from the 12-week endpoint. HoxA9, an unrelated developmental gene, is a known target of EZH2. Whereas BPH1-GFP and BPH1-Ras tumors showed no change in HoxA9 transcript levels, BPH1-EZH2 tumors showed a marked decrease in HoxA9 expression (Fig. 5E). Interestingly, in agreement with reports of Akt's negative regulation of EZH2 function (48), BPH1-Akt tumors showed a significant increase in HoxA9 expression (Fig. 5E). EZH2 was also found to regulate adrenergic receptor β-2 (ADRB2), which in turn regulates the adhesion molecules β-catenin and integrin β_4 (49). The connection between EZH2 and ADRB2 regulation provides a plausible mechanism

for EZH2-mediated cancer aggression. qRT-PCR was done to examine ADRB2 levels in the BPH1 tumors. As with HoxA9, ADRB2 levels decreased with increased EZH2 activity and increased with decreased EZH2 activity (Fig. 5F). However, changes in ADRB2 expression were not as dramatic as those seen for HoxA9.

When tumors were removed, it was noted that BPH1-Ras and BPH1-Akt tumors were more vascularized than EZH2-transformed BPH1 tumors (data not shown). Therefore, qRT-PCR was done to evaluate the levels of vascular endothelial growth factor (VEGF)-A (Fig. 5G). Consistent with the visual inspection, elevated levels of VEGF-A mRNA were observed in the BPH1-Ras and BPH1-Akt samples but not in BPH1-EZH2 (Fig. 5G). This finding suggests that the failure of the BPH1-EZH2 tumors to recruit and establish adequate vasculature resulted in the very slow growth of these tumors. Consequently, BPH1-EZH2 cells were additionally transduced with a VEGF-A-expressing lentivirus to stimulate angiogenesis. BPH1-EZH2/VEGF-A tumors grew significantly faster than BPH1-EZH2 tumors, whereas there was no change in the behavior of the control BPH1-GFP/VEGF-A tumors (Fig. 5B and C). In addition, BPH1-EZH2/VEGF-A tumors were significantly larger by mass than BPH1-GFP/VEGF-A tumors ($P = 0.002$; Fig. 5D; Table 2). Clear differences in vasculature were evident between BPH1-EZH2 and BPH1-EZH2/VEGF-A tumors on tumor excision (Supplementary Fig. S4) and confirmed by histologic evaluation (Fig. 5H; Supplementary Fig. S5). Most importantly, once neovascularization was induced in the BPH1-EZH2 tumors through VEGF-A expression, the EZH2-transformed BPH1 grew faster than BPH1-Akt tumors but slower than BPH1-Ras tumors (Fig. 5B). These data confirm the transforming ability of EZH2 and suggest that EZH2 is a stronger transforming factor than Akt but a weaker transforming factor than Ras.

Discussion

In this study, EZH2 overexpression was sufficient to transform the prostate epithelial cell line BPH1 in both *in vitro* and *in vivo* assays. EZH2 was determined to be a stronger transforming factor than constitutively active, myristoylated Akt but a weaker transforming factor than constitutively active Ras(V12). This study marks the first demonstration of EZH2-mediated neoplastic transformation of a prostate cell line. Furthermore, this is the first direct comparison between EZH2 and other, more classic oncogenes to score the strength of EZH2 as a transforming factor. EZH2 overexpression also produced an invasive phenotype in BPH1 cells, indicating that EZH2 alone is likely sufficient to promote prostate cancer aggression. EZH2 tumors, however, were poorly vascularized and grew very slowly. This phenotype was relieved by coexpression of VEGF-A, with the result of very rapid EZH2-mediated BPH1 tumor formation.

It has been well established that EZH2 is overexpressed in numerous cancer types and that its overexpression correlates with a more metastatic phenotype. A great deal of evidence has been accumulating on the mechanism by which EZH2 becomes overexpressed in cancers. EZH2 gene expression was shown to be regulated by the Rb-E2F pathway, $p16^{INK4a}$, by p53 (50-53), and most recently by microRNA-mediated repression (21), all of which are interrupted or damaged in most cancers. Therefore, EZH2 expression may increase due to loss of negative regulation by these pathways. However, the vast majority of cancers have lost functionality of p53 and Rb and only a minority of cancers overexpress EZH2. Alternatively, *in situ* hybridization experiments on late-stage prostate cancer samples revealed amplification of the EZH2 gene locus that correlates with EZH2 overexpression and cancer aggression (20). Although our system uses an artificial overexpression system, the end result of lentiviral gene introduction mimics the gene duplication observed in late-stage prostate cancer. It is, therefore, a relevant model in which to study the effects of EZH2 overexpression on prostate cancer initiation.

Although EZH2 caused the transformation and invasion of the prostate epithelial cell line BPH1, it failed to change the proliferation rate. One study knocked down EZH2 using RNA interference and saw a decrease in the proliferation rate,

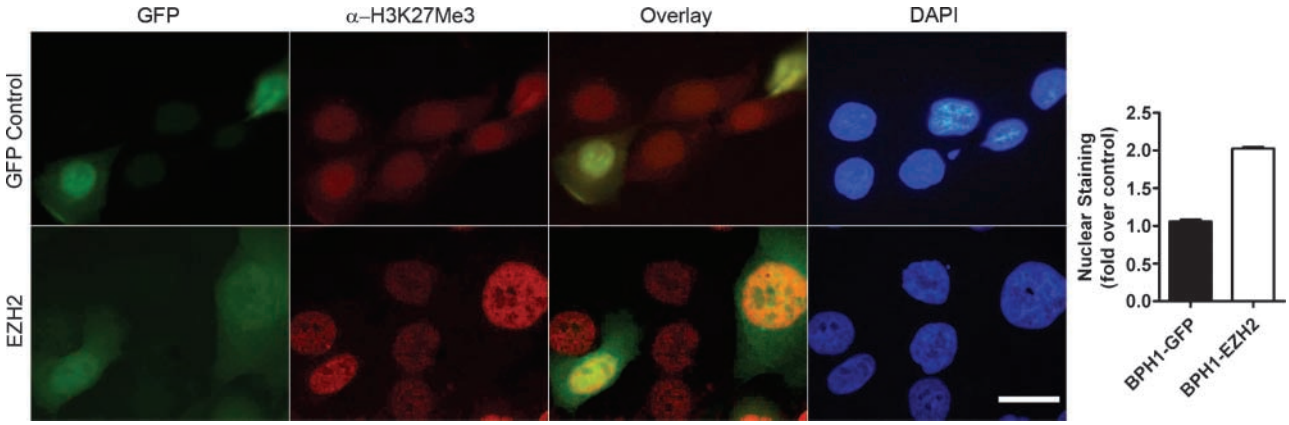

FIGURE 2. Immunocytochemistry confirmed increase in histone 3 lysine 27 trimethylation in EZH2-overexpressing BPH1. BPH1-EZH2 and BPH1-GFP were grown and fixed on coverslips and then stained with an anti-histone 3 lysine 27 trimethylation antibody (α-H3K27Me3). GFP panel shows EGFP expression in transduced cells. α-H3K27Me3 panel shows staining for trimethylation on histone 3 at lysine 27. Overlay panel allows direct comparison of GFP and H3K27Me3 panels. 4′,6-Diamidino-2-phenylindole panel shows all cells within the field of view. Bar, 25 μm. Nuclear staining intensity was quantified in GFP-positive and GFP-negative cells in each field. Fold change was calculated by average nuclear intensity of GFP-positive cells divided by average nuclear intensity of GFP-negative cells.

concluding that EZH2 was critical for cell proliferation (25). However, the same study attempted to overexpress EZH2 in prostate cancer cell lines and failed to see an increase in proliferation rate. Considering that EZH2 controls expression levels of various cell cycle genes such as cyclin A and $p16^{INK4a}$ (54, 55), one would expect that overexpressing EZH2 would result in a significant effect on cellular proliferation. Instead, it would seem that EZH2 is necessary to maintain existing cellular proliferation but is not sufficient to boost proliferation beyond the existing rate. Further investigation is needed to elucidate the mechanisms at work in regulating the cell cycle in the presence of EZH2 overexpression.

Recent studies provided some insight into possible mechanisms of EZH2-mediated transformation. EZH2 was found to regulate actin polymerization in prostate cancer cells (56), implying a system whereby EZH2 could provoke an increase in cell motility. EZH2 was also found to regulate ADBR2 in prostate cancer cells, which in turn regulates various adhesion molecules. Knocking down EZH2 in prostate cancer cell lines restored levels of ADRB2 and subsequently decreased invasive behavior (49). The observed down-regulation of ADRB2 in our BPH1-EZH2 tumor model is consistent with the proposed mechanism of EZH2. Furthermore, EZH2 was found to negatively regulate the expression of $p16^{INK4a}$ through Rb(2) (57). As p16 is a critical gene in G_1-S cell cycle control, this down-regulation by EZH2 is a possible step toward the transformation of benign cells. Interestingly, because expression levels of EZH2 are negatively regulated by $p16^{INK4a}$ through E2F, this down-regulation also creates a positive feedback loop by which EZH2 up-regulates its own expression (10, 50, 52). Although, in normal cells, EZH2 expression should be controlled through Rb and p53, this regulation may be dysfunctional in our system because BPH1 cells were immortalized using SV40 large T antigen, which antagonizes both proteins (28). The loss of active p53 through the large T antigen, combined with loss of $p16^{INK4a}$ expression initiated by the overexpression of exogenous EZH2, could explain how BPH1 cells were susceptible to transformation by EZH2. The question then remains whether EZH2 overexpression alone is adequate to drive tumor formation as a single hit or if EZH2 overexpression must be combined with other mutations in a multiple hit model to result in transformation. Additional studies examining the effects of EZH2 overexpression in primary prostate cells will be beneficial to further elucidate this issue.

A similar study on the transforming capabilities of EZH2 was done in the immortalized breast epithelial cell line H16N2 (26). These cells were immortalized by human papillomavirus 16, which acts through the E6 and E7 genes to bind to and inhibit both Rb and p53 and thus present a similar system to the BPH1 cell line presented here. In the breast study, EZH2 was overexpressed through an adenoviral vector and shown to increase invasive behavior and soft-agar colony formation. However, this study did not pursue the question of *in vivo* transformation through a tumor growth assay. This may have been due to the limitation presented by adenoviral-mediated overexpression of EZH2. Our study was able to present the tumorigenic properties of EZH2 in the context of *in vivo* tumor growth because the lentiviral overexpression vector permanently and stably expressed EZH2. This contributes a valuable and previously unpublished aspect of EZH2 transformation capabilities. Furthermore, because of the tissue-specific characteristics unique to breast and prostate tissues and the resulting signaling differences that must result from these characteristics, we considered it prudent to address the issue of EZH2-mediated neoplastic transformation directly in prostate cells rather than through inference because hormone receptor signaling may alter the effect of the overexpressed gene.

EZH2 overexpression has been repeatedly implicated in the aggressive behavior of prostate and numerous other cancers. Here, we have shown that EZH2 overexpression may also be responsible for the initiating events of prostate cancer. It is critical that the effect of EZH2 overexpression in prostate tissue continues to be explored. Only a more thorough understanding of tissue-specific protein behavior will facilitate the development of treatments that can specifically target the aggressive subset of EZH2-overexpressing tumors.

Materials and Methods

Constructs

Lentiviruses were constructed in pCCL (58). HA-EZH2 (59) was inserted into pCCL-CMV-IRES-EGFP to create pCCL-CMV-EZH2-IRES-EGFP. Empty vector was used as GFP control.

pCCL-CMV-RLuc (60), pCCL-CMV-VEGF-A-IRES-EGFP (60), pRRL-CMV-Ras(V12)-IRES-EGFP (47), and FUW-Akt-IRES-GFP (46) were described previously.

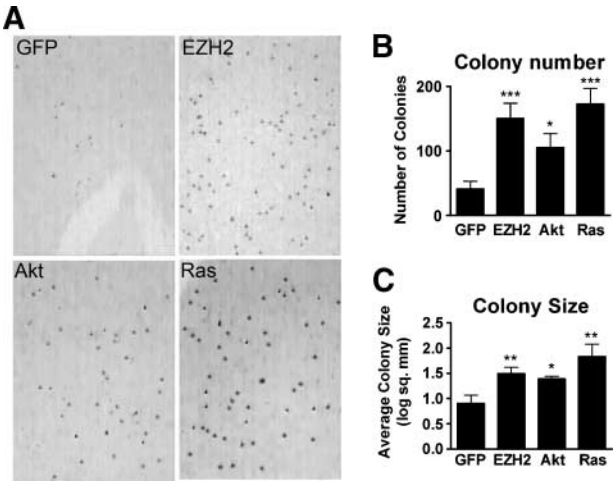

FIGURE 3. EZH2 overexpression was sufficient to transform BPH1 cells. BPH1 cells were marked with GFP, EZH2, Akt, or Ras(V12) lentivirus. **A.** Soft-agar colony growth assay with all BPH1 sublines. EZH2 overexpression by lentiviral transduction was sufficient to cause transformation of BPH1 cells. BPH1 cells infected with the classic oncogenes Akt and Ras served as positive controls for colony formation. **B.** Soft-agar growth results plotted by colony number alone. BPH1-GFP control grew very few colonies. BPH1-Akt ($P = 0.02$) showed mild colony formation, BPH1-Ras ($P = 0.00019$) showed stronger colony formation, and BPH1-EZH2 ($P = 0.00081$) fell directly between the two. **C.** Soft-agar growth results plotted by colony size. BPH1-Akt ($P = 0.0247$), BPH1-Ras ($P = 0.004$), and BPH1-EZH2 ($P = 0.0087$). *, $P < 0.05$; **, $P < 0.01$; ***, $P < 0.001$, relative to BPH1-GFP control (Student's *t* test). Results of four independent experiments.

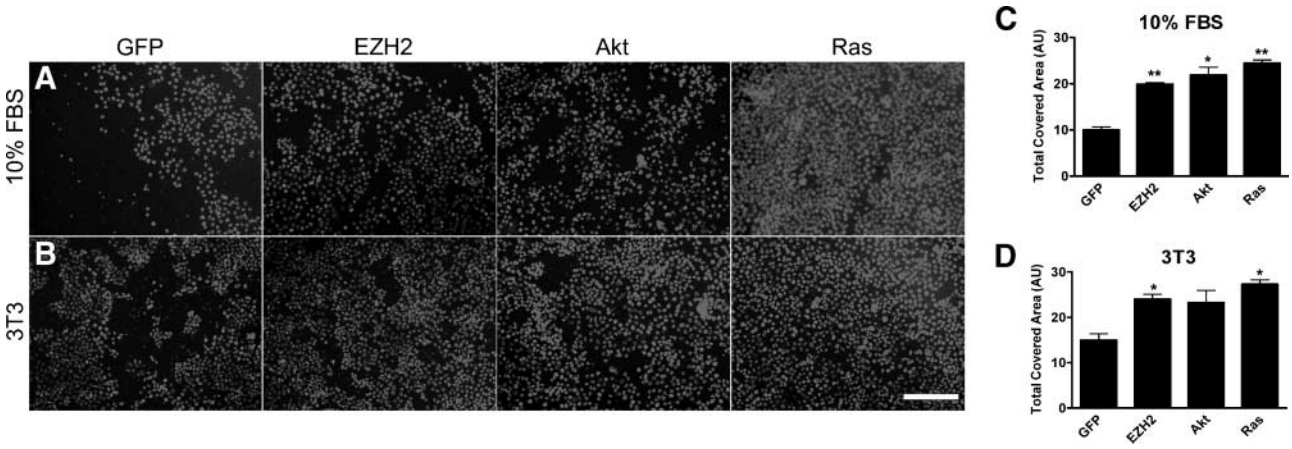

FIGURE 4. Overexpression of EZH2 increased invasive behavior of BPH1 cells. BPH1 sublines were assayed for invasive behavior toward either (**A**) 10% FBS-containing medium or (**B**) 3T3 conditioned serum-free medium. Cells were allowed to invade for 48 h through a Matrigel-coated 8 μm membrane and then fixed and stained with 4′,6-diamidino-2-phenylindole. Assays were done in duplicate. Bar, 100 μm. **C.** Quantification of cells invaded toward 10% FBS-containing medium by total membrane area covered. **D.** Quantification of cells invaded toward 3T3-containing medium by total membrane area covered. *, $P < 0.05$; **, $P < 0.01$. AU, arbitrary units. All statistical analyses were done using Student's *t* test against BPH1-GFP control values.

Tissue Culture

Cells were cultured in medium with 10% FBS and 1% penicillin-streptomycin at 37°C with 5% CO_2 and humidity. HEK-283T cells were cultured in Iscove's modification of DMEM with L-glutamine and 25 mmol/L HEPES without α-thioglycerol and β-mercaptoethanol. 3T3 cells were cultured in DMEM with 4.5 g/L glucose, L-glutamine, and sodium pyruvate. BPH1 cells were cultured in RPMI 1640 with L-glutamine (Mediatech).

Lentivirus was produced by triple transfections into HEK-293T cells using calcium phosphate transfection protocol (61).

Lentiviral transductions were done at a multiplicity of infection of 1 for 6 h with 8 μg/mL polybrene (Sigma). On day 4, transduced cells were assayed for lentiviral gene expression and seeded for additional assays.

Viable cells were measured by the formazan dye–based CCK8 assay. Briefly, cells were plated in triplicate on day 0 at 1×10^3 per well in 100 μL medium in a 96-well plate. On days 1, 3, and 5, 10 μL CCK8 assay reagent (Dojindo) was added to the wells and incubated for 2 h. Plates were read at an absorbance of 450 nm on a Bio-Tek PowerwaveXS Plate Reader (Bio-Tek) and analyzed using KC Junior Software (Bio-Tek). Apoptotic cells were measured by lactase dehydrogenase assay according to the manufacturer's protocol (Takara Bio).

Western Blot

Samples were lysed in Whole-Cell Lysis Buffer [50 mmol/L HEPES, 150 mmol/L NaCl, 1.5 mmol/L $MgCl_2$, 0.5 mmol/L EDTA, 10% glycerol, 1% Triton X-100, 10 mmol/L NaF, 1 mmol/L DTT, 1 mmol/L phenylmethylsulfonyl fluoride (pH 7.0)] by three freeze-thaw cycles followed by 30 min on ice. Lysates were spun down at $4,000 \times g$ for 5 min, and supernatants were transferred to clean tubes. Total protein (25 μg/sample) was separated by electrophoresis on 4% to 20% Tris-HCl SDS-PAGE. Antibodies used are as follows: horseradish peroxidase–conjugated anti-HA (1:100; Roche), anti-EZH2 (1:500; Upstate), anti-GFP (1:1,000; Invitrogen), anti-β-actin (1:5,000; Sigma), horseradish peroxidase–conjugated anti-rabbit (1:20,000; Santa Cruz Biotechnology), and horseradish peroxidase–conjugated anti-mouse (1:20,000; Santa Cruz Biotechnology). Quantification of Western blots was done by densitometry using ImageJ.

Microscopy

All cells and tissues were photographed using an Olympus BX41 fluorescent microscope (Olympus) fitted with a Q-Imaging QICAM FAST 1394 camera (Surrey). Images were captured using the software QCapture Pro Version 5.1 (Media Cybernetics) and processed using Adobe Photoshop CS (Adobe Systems) or ImageJ.

Immunocytochemistry and Immunohistochemistry

Cells for immunocytochemistry were plated at 2.5×10^5 on growth-treated, sterile glass coverslips in a 6-well plate (62) and allowed to attach and grow for 36 h. Coverslips were washed in PBS-CM (PBS with 100 μmol/L $CaCl_2$ and 1 mmol/L $MgCl_2$) and fixed in 3% paraformaldehyde in PBS-CM for 20 min at room temperature. Cells were permeabilized for 5 min in 3% paraformaldehyde in PBS-CM with 0.1% Triton X-100 and washed three times in PBS with 0.5% bovine serum albumin. Coverslips were blocked for 20 min at room temperature in PBS with 3% bovine serum albumin and 1% normal goat serum.

Table 1. Quantification of Invasion by BPH1 Sublines

Sample	Total Area ± SD (AU)	*P**
10% FBS		
GFP	10.006 ± 0.907	N/A
EZH2	19.918 ± 0.428	0.005
Akt	21.923 ± 2.34	0.021
Ras	24.481 ± 0.968	0.004
3T3		
GFP	14.976 ± 1.981	N/A
EZH2	24.039 ± 1.474	0.035
Akt	23.241 ± 3.839	0.114
Ras	27.306 ± 1.439	0.035

**P* values determined using Student's *t* test against GFP control values.

Antibodies were diluted in PBS with 0.1% bovine serum albumin and 1% normal goat serum. Coverslips were incubated in a humidity chamber with antibody overnight at 4°C. Coverslips were mounted on a glass slide using Vectashield Hardmount with 4′,6-diamidino-2-phenylindole (Vector Labs). Antibodies used were anti-histone 3 lysine 27 trimethylation (1:750; Upstate) and Alexa Fluor 594 $F(ab')_2$ fragment of goat anti-mouse IgG (1:1,000; Invitrogen). Images shown in Fig. 2 were captured using a ×40 objective lens.

Tumors (1 cm) used for immunohistochemistry were fixed overnight in 3% paraformaldehyde at 4°C followed by 5 min of washing and storage in 50% ethanol. Tissues were embedded in paraffin and sectioned at the University of California at Los Angeles (UCLA) Translational Pathology Core Laboratory. Sections were subsequently processed as described previously (63). Antibodies used were biotinylated anti-CD31 (1:300; BD Pharmingen), anti-GFP (1:100; Invitrogen), anti-HA (1:100; Roche), biotinylated anti-rabbit (1:100; Vector Labs), biotinylated anti-rat (1:100; Vector Labs), streptavidin-horseradish peroxidase (1:100; Perkin-Elmer), streptavidin-Cy3 (The Jackson Laboratory), and streptavidin-FITC (1:100; Invitrogen). Images shown in Fig. 5 and Supplementary Fig. S4 were captured using a ×4 or ×10 objective lens.

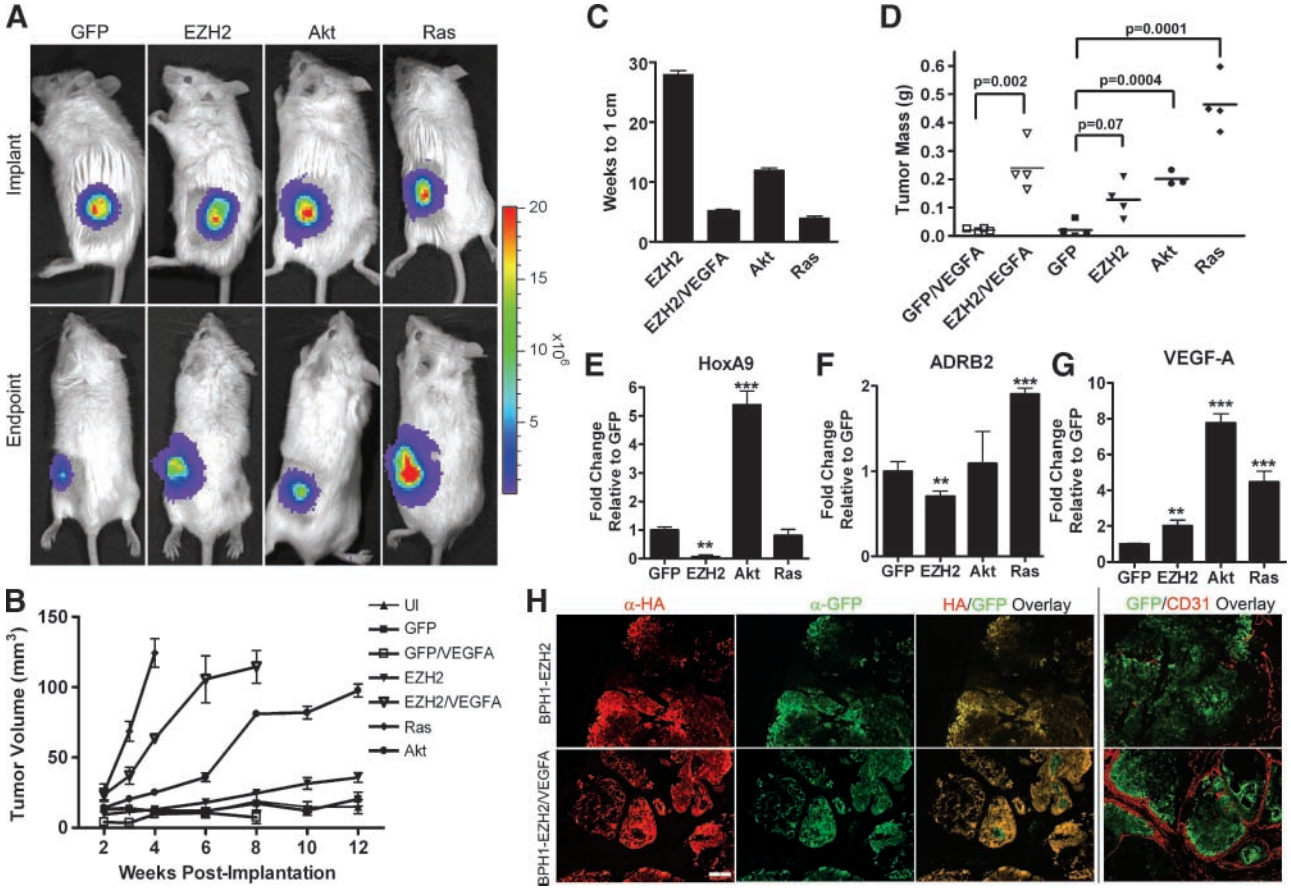

FIGURE 5. EZH2-mediated transformation of BPH1 cell line resulted in tumor growth in severe combined immunodeficient mice. BPH1 sublines were implanted in the flanks of severe combined immunodeficient mice. **A.** Equivalent numbers of cells, confirmed by comparable optical signal, were implanted for each group on day 0. Differences in optical signal at study endpoint showed differential tumor growth rates among the groups. **B.** Physical caliper measurements showed rapid growth by Ras tumors and slower growth by Akt tumors. BPH1-EZH2 (EZH2) tumors grew very slowly due to limited vasculature and nutrient delivery but still grew relative to uninfected BPH1 (*UI*), BPH1-GFP (*GFP*), and BPH1-GFP/VEGF-A (*GFP/VEGF-A*) controls. When angiogenesis was stimulated by VEGF-A expression, BPH1-EZH2/VEGF-A (*EZH2/VEGF-A*) tumors grew faster than BPH1-Akt (Akt) but slower than BPH1-Ras (Ras). **C.** Time required for each BPH1 tumor type to reach 1 cm radius. **D.** BPH1-Ras tumors were largest at excision and BPH1-Akt tumors were smaller. Poorly vascularized BPH1-EZH2 tumors were smaller than BPH1-Akt, but well-vascularized BPH1-EZH2/VEGF-A tumors were much larger than BPH1-Akt. Tumor mass at removal confirmed expansion of BPH1-Ras ($P = 0.0002$), BPH1-Akt ($P = 0.001$), BPH1-EZH2 ($P = 0.03$), and BPH1-EZH2/VEGF-A ($P = 0.002$) but not BPH1-GFP and BPH1-GFP/VEGF-A cells *in vivo*. qRT-PCR on extracted tumors for (**E**) HoxA9, (**F**) ADRB2, and (**G**) VEGF-A. **E.** Changes in HoxA9 expression corresponded with increased (BPH1-EZH2, 0.5-fold of BPH1-GFP, $P = 0.0006$) or decreased (BPH1-Akt, 5.4-fold of BPH1-GFP, $P = 1.8 \times 10^{-7}$) EZH2 activity. **F.** Changes in ADBR2 expression corresponded with increased (BPH1-EZH2, 0.7-fold of BPH1-GFP, $P = 0.0003$) or decreased (BPH1-Akt, 1.2-fold of BPH1-GFP, $P = 0.46$) EZH2 activity. **G.** Differences in observed tumor vasculature at excision were corroborated by differences in VEGF-A expression (BPH1-EZH2, $P = 0.01$; BPH1-Akt, $P = 1.0 \times 10^{-7}$; BPH1-Ras, $P = 0.0002$). *, $P < 0.05$; **, $P < 0.01$; ***, $P < 0.001$, relative to GFP control (Student's *t* test). **H.** BPH1-EZH2 and BPH1-EZH2/VEGF-A tumors stained for exogenous EZH2 expression (HA), GFP, and vasculature (CD31). GFP expression is indicative of cells transduced with either EZH2 or VEGF-A virus (in BPH1-EZH2/VEGF-A sample) and overlays with HA expression. CD31 expression on vasculature is greatly increased in the BPH1-EZH2/VEGF-A tumor compared with the BPH1-EZH2 tumor. Additional panels are shown in Supplementary Fig. S4. Bar, 200 μm.

Table 2. *P* values for BPH1 Tumor Measurements

	P values*					
	Wk 2	Wk 4	Wk 6	Wk 8	Wk 10	Wk 12
EZH2	0.176	0.555	0.045	0.010	0.019	0.021
EZH2/VEGF-A	0.002	8.2E-09	0.001	2.3E-04	—	—
Akt	0.754	0.001	4.3E-04	3.8E-06	2.2E-04	3.1E-04
Ras	0.134	3.3E-05	—	—	—	—

**P* values determined using Student's *t* test against GFP control values.

Matrigel Invasion Assay

The invasion assay protocol was adapted from previously reported studies (64). Briefly, 24-well plate inserts with 8 μm membrane pores (BD Falcon) were coated evenly with 20 μL of 1:6 Matrigel/serum-free medium dilution (BD Biosciences) and then allowed to set for 30 min at 37°C. Cells (1×10^5) were plated in the top chamber in 500 μL medium containing 0.5% FBS. The bottom chamber was filled with 500 μL of either medium containing 10% FBS or 3T3 conditioned serum-free medium. Cells were allowed to invade for 48 h.

Invaded cells were fixed in 0.5% glutaraldehyde in 1× Dulbecco's PBS for 20 min, and the Matrigel layer was removed with a cotton swab. The membrane was cut out of the chamber using a no. 11 scalpel blade and mounted on a slide under a coverslip using Vectashield Hardmount with 4′,6-diamidino-2-phenylindole (Vector Labs). Each membrane was quantified by capturing five independent fields under the ×10 lens of the Olympus BX41 fluorescent microscope and determining the total area covered by cells in the field using ImageJ. The five fields were combined to obtain total membrane coverage. Images shown in Fig. 4 were captured using a ×4 objective lens.

Soft-Agar Transformation Assay

The base layer was made by combining molten 1% agar equalized to 40°C with 2× RPMI 1640/20% FBS in a 1:1 dilution and plating 100 μL in each well of a 96-well plate. The base layer was allowed to set for 20 min at room temperature. Cells (5×10^3 per well) were resuspended in 25 μL of 2× RPMI 1640/20% FBS, mixed with 25 μL molten 0.7% sterile agarose equalized to 40°C, and plated on the base layer. The top layer was allowed to set for 20 min, and plates were placed at 37°C with 5% CO_2 and humidity. Colonies grew for 14 days and then stained overnight with 0.1% INT-violet dye (Sigma).

Plates were assayed at the UCLA Immunology Core on an Immunospot Series 1 Imager (Cellular Technologies). Colonies were photographed, analyzed, and counted using ImmunoSpot 4.0 Professional by CTL.

Animal Work and Optical Imaging

Animal care and procedures were done in accordance with the University of California Animal Research Committee guidelines. Age-matched male severe combined immunodeficient mice from Charles Rivers were used. Mice were implanted on the flank with 1×10^6 BPH1 cells marked with each respective lentivirus (at a multiplicity of infection of 3) and subsequently with RLuc lentivirus (at a multiplicity of infection of 1). For BPH1-EZH2/VEGF-A and BPH1-GFP/VEGF-A tumors, the original cultures of BPH1-EZH2 or BPH1-GFP cells were additionally marked with pCCL-CMV-VEGF-A-IRES-EGFP lentivirus at a multiplicity of infection of 1. These cells were not marked with pCCL-RLuc, so the overall lentiviral load on the cells remained unchanged from the original groups.

For each imaging session, mice were anesthetized with ketamine/xylazine (4:1). *In vivo* luciferase expression was monitored over time using a cooled IVIS CCD camera (Xenogen). Mice were given a tail-vein injection of coelenterazine at a dose of 1 mg/kg for RLuc imaging. Images were analyzed with IGOR-PRO Living Image Software (Xenogen). Tumor volumes were calculated using the formula: $V = a \times 2b \times \pi / 6$, where a is the largest diameter and b is the smallest diameter (65, 66). All animals were sacrificed when the largest diameter of the tumor reached 10 mm or at 12 weeks post-implantation. On removal, tumors were harvested and snap frozen in liquid nitrogen to preserve RNA integrity or fixed in 3% paraformaldehyde overnight for histology.

RNA Extraction and qRT-PCR

RNA was extracted using TRIzol reagent (Invitrogen). RNA (2 μg) was reverse transcribed using iScript cDNA Synthesis Kit (Bio-Rad). qRT-PCR was done using 1 μL cDNA (~40 ng), SYBR Green 2× master mix (Applied Biosystems), 10 nmol/L fluorescein, and 10 μmol/L each of the following primers: β-actin 5′-TCAAGATCATTGCTCCTCCTGAGC-3′ and 5′-TACTCCTGCTTGCTGATCCACATC-3′, EZH2 5′-AGCGGATAAAGACCCCACC-3′ and 5′-CTGCTTCCCTATCACTGTC-3′, EED 5′-GTAGAAGGGCACAGAGATG-3′ and 5′-GGCCTGTTAGTTTTATTTGG-3′, HoxA9 5′-TGCAGCTTCCAGTCCAAGG-3′ and 5′-GTAGGGGTGGTGGTGATGGT-3′, ADRB2 5′-TTCACGAACCAAGCCTATGCCA-3′ and 5′-AGCGGCCCTCAGATTTGTCAAT-3′, and VEGF-A 5′-TGTACCTCCACCATGCCAAGT-3′ and 5′-CGCTGGTAGACGTCCATGAA-3′.

Reactions were run on MyiQ iCycler RT-PCR machine (Bio-Rad) under the following cycling conditions: 40 repeats of 95°C of 15 s, 60°C for 30 s, and 72°C for 30 s, and analyzed using Bio-Rad iQ5 software. All samples were normalized to internal β-actin levels by the comparative threshold cycle (Ct) method (67).

Disclosure of Potential Conflicts of Interest

No potential conflicts of interest were disclosed.

Acknowledgments

We thank Drs. Simon Hayward, Lee Slice, and Li Xin for generous contributions of BPH1 cell line, pRRL-CMV-Ras(V12)-IRES-EGFP, and FUW-Akt-IRES-GFP, respectively, and Drs. Maarten van Lohuizen and Thomas Jenuwein for supplying the initial HA-tagged EZH2 construct.

Flow cytometry was done at the UCLA Jonsson Comprehensive Cancer Center and Center for AIDS Research Flow Cytometry Core Facility, which is supported by the NIH awards CA-16042 and AI-28697, Jonsson Cancer Center, UCLA AIDS Institute, and UCLA School of Medicine. BioSpot was done at the UCLA Immuno/BioSpot Core Facility, which is supported by the UCLA Center for AIDS Research, NIH/National Institute of Allergy and Infectious Diseases grant AI028697, and David Geffen School of Medicine at UCLA.

References

1. Brock HW, van Lohuizen M. The polycomb group—no longer an exclusive club? Curr Opin Genet Dev 2001;11:175–81.

2. Orlando V. Polycomb, epigenomes, and control of cell identity. Cell 2003;112: 599–606.

3. Cao R, Zhang Y. SUZ12 is required for both the histone methyltransferase activity and the silencing function of the EED-EZH2 complex. Mol Cell 2004; 15:57–67.

4. Sewalt RG, van der Vlag J, Gunster MJ, et al. Characterization of interactions between the mammalian polycomb-group proteins Enx1/EZH2 and EED suggests the existence of different mammalian polycomb-group protein complexes. Mol Cell Biol 1998;18:3586–95.

5. Bunker CA, Kingston RE. Transcriptional repression by *Drosophila* and mammalian polycomb group proteins in transfected mammalian cells. Mol Cell Biol 1994;14:1721–32.

6. Cao R, Wang L, Wang H, et al. Role of histone H3 lysine 27 methylation in polycomb-group silencing. Science 2002;298:1039–43.

7. Kirmizis A, Bartley SM, Kuzmichev A, et al. Silencing of human polycomb target genes is associated with methylation of histone H3 Lys 27. Genes Dev 2004;18:1592–605.

8. Cao R, Zhang Y. The functions of E(Z)/EZH2-mediated methylation of lysine 27 in histone H3. Curr Opin Genet Dev 2004;14:155–64.

9. Jenuwein T, Allis CD. Translating the histone code. Science 2001;293: 1074–80.

10. Muller J, Hart CM, Francis NJ, et al. Histone methyltransferase activity of a *Drosophila* polycomb group repressor complex. Cell 2002;111:197–208.

11. Visser HP, Gunster MJ, Kluin-Nelemans HC, et al. The polycomb group protein EZH2 is upregulated in proliferating, cultured human mantle cell lymphoma. Br J Haematol 2001;112:950–8.

12. Varambally S, Dhanasekaran SM, Zhou M, et al. The polycomb group protein EZH2 is involved in progression of prostate cancer. Nature 2002;419:624–9.

13. Collett K, Eide GE, Arnes J, et al. Expression of enhancer of zeste homologue 2 is significantly associated with increased tumor cell proliferation and is a marker of aggressive breast cancer. Clin Cancer Res 2006;12:1168–74.

14. Raaphorst FM, Meijer CJ, Fieret E, et al. Poorly differentiated breast carcinoma is associated with increased expression of the human polycomb group EZH2 gene. Neoplasia 2003;5:481–8.

15. Bachmann IM, Halvorsen OJ, Collett K, et al. EZH2 expression is associated with high proliferation rate and aggressive tumor subgroups in cutaneous melanoma and cancers of the endometrium, prostate, and breast. J Clin Oncol 2006;24: 268–73.

16. McHugh JB, Fullen DR, Ma L, Kleer CG, Su LD. Expression of polycomb group protein EZH2 in nevi and melanoma. J Cutan Pathol 2007;34:597–600.

17. Croonquist PA, Van Ness B. The polycomb group protein enhancer of zeste homolog 2 (EZH 2) is an oncogene that influences myeloma cell growth and the mutant ras phenotype. Oncogene 2005;24:6269–80.

18. Mattioli E, Vogiatzi P, Sun A, et al. Immunohistochemical analysis of pRb2/p130, VEGF, EZH2, p53, p16(INK4A), p27(KIP1), p21(WAF1), Ki-67 expression patterns in gastric cancer. J Cell Physiol 2007;210:183–91.

19. Gil J, Bernard D, Peters G. Role of polycomb group proteins in stem cell self-renewal and cancer. DNA Cell Biol 2005;24:117–25.

20. Saramaki OR, Tammela TL, Martikainen PM, Vessella RL, Visakorpi T. The gene for polycomb group protein enhancer of zeste homolog 2 (EZH2) is amplified in late-stage prostate cancer. Genes Chromosomes Cancer 2006;45:639–45.

21. Varambally S, Cao Q, Mani RS, et al. Genomic loss of microRNA-101 leads to overexpression of histone methyltransferase EZH2 in cancer. Science 2008; 322:1695–9.

22. Laitinen S, Martikainen PM, Tolonen T, et al. EZH2, Ki-67 and MCM7 are prognostic markers in prostatectomy treated patients. Int J Cancer 2008;122: 595–602.

23. Rhodes DR, Sanda MG, Otte AP, Chinnaiyan AM, Rubin MA. Multiplex biomarker approach for determining risk of prostate-specific antigen-defined recurrence of prostate cancer. J Natl Cancer Inst 2003;95:661–8.

24. Yu J, Yu J, Rhodes DR, et al. A polycomb repression signature in metastatic prostate cancer predicts cancer outcome. Cancer Res 2007;67:10657–63.

25. Bryant RJ, Cross NA, Eaton CL, Hamdy FC, Cunliffe VT. EZH2 promotes proliferation and invasiveness of prostate cancer cells. Prostate 2007;67:547–56.

26. Kleer CG, Cao Q, Varambally S, et al. EZH2 is a marker of aggressive breast cancer and promotes neoplastic transformation of breast epithelial cells. Proc Natl Acad Sci U S A 2003;100:11606–11.

27. Wissmann M, Yin N, Muller JM, et al. Cooperative demethylation by JMJD2C and LSD1 promotes androgen receptor-dependent gene expression. Nat Cell Biol 2007;9:347–53.

28. Hayward SW, Dahiya R, Cunha GR, et al. Establishment and characterization of an immortalized but non-transformed human prostate epithelial cell line: BPH-1. In Vitro Cell Dev Biol Anim 1995;31:14–24.

29. Mitchell S, Abel P, Ware M, Stamp G, Lalani E. Phenotypic and genotypic characterization of commonly used human prostatic cell lines. BJU Int 2000;85: 932–44.

30. Untergasser G, Rumpold H, Hermann M, et al. Proliferative disorders of the aging human prostate: involvement of protein hormones and their receptors. Exp Gerontol 1999;34:275–87.

31. Phillips JL, Hayward SW, Wang Y, et al. The consequences of chromosomal aneuploidy on gene expression profiles in a cell line model for prostate carcinogenesis. Cancer Res 2001;61:8143–9.

32. Shou J, Soriano R, Hayward SW, et al. Expression profiling of a human cell line model of prostatic cancer reveals a direct involvement of interferon signaling in prostate tumor progression. Proc Natl Acad Sci U S A 2002;99:2830–5.

33. Cunha GR, Hayward SW, Wang YZ. Role of stroma in carcinogenesis of the prostate. Differentiation 2002;70:473–85.

34. Majumder PK, Sellers WR. Akt-regulated pathways in prostate cancer. Oncogene 2005;24:7465–74.

35. Manning BD, Cantley LC. AKT/PKB signaling: navigating downstream. Cell 2007;129:1261–74.

36. Majumder PK, Yeh JJ, George DJ, et al. Prostate intraepithelial neoplasia induced by prostate restricted Akt activation: the MPAKT model. Proc Natl Acad Sci U S A 2003;100:7841–6.

37. Sansom OJ, Meniel V, Wilkins JA, et al. Loss of Apc allows phenotypic manifestation of the transforming properties of an endogenous K-ras oncogene *in vivo*. Proc Natl Acad Sci U S A 2006;103:14122–7.

38. Bos JL. ras oncogenes in human cancer: a review. Cancer Res 1989;49: 4682–9.

39. Malumbres M, Barbacid M. RAS oncogenes: the first 30 years. Nat Rev Cancer 2003;3:459–65.

40. Rosen DG, Yang G, Bast RC, Jr., Liu J. Use of ras-transformed human ovarian surface epithelial cells as a model for studying ovarian cancer. Methods Enzymol 2005;407:660–76.

41. Traynor P, McGlynn LM, Mukhergee R, et al. An increase in N-Ras expression is associated with development of hormone refractory prostate cancer in a subset of patients. Dis Markers 2008;24:157–65.

42. Bakin RE, Gioeli D, Sikes RA, Bissonette EA, Weber MJ. Constitutive activation of the Ras/mitogen-activated protein kinase signaling pathway promotes androgen hypersensitivity in LNCaP prostate cancer cells. Cancer Res 2003;63: 1981–9.

43. Weber MJ, Gioeli D. Ras signaling in prostate cancer progression. J Cell Biochem 2004;91:13–25.

44. Chen H, Tu SW, Hsieh JT. Down-regulation of human DAB2IP gene expression mediated by polycomb Ezh2 complex and histone deacetylase in prostate cancer. J Biol Chem 2005;280:22437–44.

45. Miyoshi H, Blomer U, Takahashi M, Gage FH, Verma IM. Development of a self-inactivating lentivirus vector. J Virol 1998;72:8150–7.

46. Xin L, Lawson DA, Witte ON. The Sca-1 cell surface marker enriches for a prostate-regenerating cell subpopulation that can initiate prostate tumorigenesis. Proc Natl Acad Sci U S A 2005;102:6942–7.

47. Pham H, Eibl G, Vincenti R, et al. 15-Hydroxyprostaglandin dehydrogenase suppresses K-RasV12-dependent tumor formation in *nu/nu* mice. Mol Carcinog 2008;47:466–77.

48. Cha TL, Zhou BP, Xia W, et al. Akt-mediated phosphorylation of EZH2 suppresses methylation of lysine 27 in histone H3. Science 2005;310:306–10.

49. Yu J, Cao Q, Mehra R, et al. Integrative genomics analysis reveals silencing of β-adrenergic signaling by polycomb in prostate cancer. Cancer Cell 2007;12: 419–31.

50. Bracken AP, Pasini D, Capra M, et al. EZH2 is downstream of the pRB-E2F pathway, essential for proliferation and amplified in cancer. EMBO J 2003;22: 5323–35.

51. Muller H, Bracken AP, Vernell R, et al. E2Fs regulate the expression of genes involved in differentiation, development, proliferation, and apoptosis. Genes Dev 2001;15:267–85.

52. Reynolds PA, Sigaroudinia M, Zardo G, et al. Tumor suppressor $p16^{INK4A}$ regulates polycomb-mediated DNA hypermethylation in human mammary epithelial cells. J Biol Chem 2006;281:24790–802.

53. Tang X, Milyavsky M, Shats I, et al. Activated p53 suppresses the histone methyltransferase EZH2 gene. Oncogene 2004;23:5759–69.

54. Attwooll C, Oddi S, Cartwright P, et al. A novel repressive E2F6 complex containing the polycomb group protein, EPC1, that interacts with EZH2 in a proliferation-specific manner. J Biol Chem 2005;280:1199–208.

55. Tonini T, Bagella L, D'Andrilli G, Claudio PP, Giordano A. Ezh2 reduces the ability of HDAC1-dependent pRb2/p130 transcriptional repression of cyclin A. Oncogene 2004;23:4930–7.

56. Bryant RJ, Winder SJ, Cross SS, Hamdy FC, Cunliffe VT. The polycomb group protein EZH2 regulates actin polymerization in human prostate cancer cells. Prostate 2008;68:255–63.

57. Kotake Y, Cao R, Viatour P, et al. pRB family proteins are required for H3K27 trimethylation and polycomb repression complexes binding to and silencing $p16^{INK4\alpha}$ tumor suppressor gene. Genes Dev 2007;21:49–54.

58. Dull T, Zufferey R, Kelly M, et al. A third-generation lentivirus vector with a conditional packaging system. J Virol 1998;72:8463–71.

59. Laible G, Wolf A, Dorn R, et al. Mammalian homologues of the polycomb-group gene enhancer of zeste mediate gene silencing in *Drosophila* heterochromatin and at *S. cerevisiae* telomeres. EMBO J 1997;16:3219–32.

60. Burton JB, Priceman SJ, Sung JL, et al. Suppression of prostate cancer nodal and systemic metastasis by blockade of the lymphangiogenic axis. Cancer Res 2008;68:7828–37.

61. Soneoka Y, Cannon PM, Ramsdale EE, et al. A transient three-plasmid expression system for the production of high titer retroviral vectors. Nucleic Acids Res 1995;23:628–33.

62. Aschenbrenner L, Lee T, Hasson T. Myo6 facilitates the translocation of endocytic vesicles from cell peripheries. Mol Biol Cell 2003;14:2728–43.

63. Brakenhielm E, Burton JB, Johnson M, et al. Modulating metastasis by a lymphangiogenic switch in prostate cancer. Int J Cancer 2007;121:2153–61.

64. Lochter A, Werb Z, Bissell MJ. Transcriptional regulation of stromelysin-1 gene expression is altered during progression of mouse mammary epithelial cells from functionally normal to malignant. Matrix Biol 1999;18:455–67.

65. Sorensen AG, Patel S, Harmath C, et al. Comparison of diameter and perimeter methods for tumor volume calculation. J Clin Oncol 2001;19:551–7.

66. Tomayko MM, Reynolds CP. Determination of subcutaneous tumor size in athymic (nude) mice. Cancer Chemother Pharmacol 1989;24:148–54.

67. Winer J, Jung CK, Shackel I, Williams PM. Development and validation of real-time quantitative reverse transcriptase-polymerase chain reaction for monitoring gene expression in cardiac myocytes *in vitro*. Anal Biochem 1999;270: 41–9.